Attribution of the Late-Twentieth-Century Rainfall Decline in Southwest Australia

BERTRAND TIMBAL

Bureau of Meteorology Research Centre, Melbourne, Australia

JULIE M. ARBLASTER

National Center for Atmospheric Research, Boulder, Colorado, and Bureau of Meteorology Research Centre, Melbourne, Australia

SCOTT POWER

Bureau of Meteorology Research Centre, Melbourne, Australia

(Manuscript received 8 February 2005, in final form 15 September 2005)

ABSTRACT

There was a dramatic decrease in rainfall in the southwest of Australia (SWA) in the mid-1960s. A statistical method, based on the idea of analogous synoptic situations, is used to help clarify the cause of the drying. The method is designed to circumvent error in the rainfall simulated directly by a climate model, and to exploit the ability of the model to simulate large-scale fields reasonably well. The method uses relationships between patterns of various atmospheric fields with station records of rainfall to improve the simulation of the local rainfall spatial variability. The original technique was developed in a previous study. It is modified here for application to two four-member ensembles of simulations of the climate from 1870 to 1999 performed with the Parallel Climate Model (PCM). The first ensemble, called "natural," is forced with natural variations in both volcanic activity and solar forcing. The second ensemble, called "full forcing," also includes three types of human-induced forcing resulting from changes in greenhouse gases, ozone, and aerosols. The full-forcing runs provide a better match to observational changes in sea surface temperature in the vicinity of SWA. The observed rainfall decline is not well captured by rainfall changes simulated directly by the model in either ensemble. There is a hint that the fully forced ensemble is more realistic, but it is nothing more than a hint. The downscaling approach, on the other hand, provides a much more accurate reproduction of the day-to-day variability of rainfall in SWA than the rainfall simulated directly by the model. The downscaled ensemble mean rainfall in full forcing declines over the region with a spatial pattern that is similar to the observed decline. This contrasts with an increase of rainfall in the downscaled rainfall in the natural ensemble. These results give the clearest indication yet that anthropogenic forcing played a role in the drying of SWA. Note, however, that ambiguities remain. For example, although the observed decline fits within the range of downscaled model simulation, the ensemble mean rainfall decline is only about half of the observed estimate, the timing differs from the observations, drying did not occur in the downscaling of one of the four full-forced ensemble members, and not all potential forcing mechanisms are included in full forcing (e.g., land surface changes). Furthermore, while the observed rainfall decline was a sharp reduction in the 1960s, followed by a near-constant rainfall regime, the full-forcing ensemble suggests a more gradual rainfall decline over 40 yr from 1960.

1. Introduction

The southwest corner of Australia (SWA) experiences a Mediterranean climate, with a relatively wet 6-month period from May to October. It is a small climatic entity, on the edge of a large dry continent. Starting in the late 1950s, SWA has experienced a dramatic rainfall decrease. The reduction occurred mostly during the 1960s and 1970s, and affected the early part of the winter rainfall from May to July. The rainfall trend is only one element of a range of climatic indices, such as sea surface temperatures (SSTs) in the south Indian Ocean or mean sea level pressure (MSLP) in Perth, Australia, that also show trends. Early studies (Nicholls 1989; Allan and Haylock 1993) have shown that these types of associations are only simultaneous and may not

Corresponding author address: Dr. B. Timbal, BMRC, GPO Box 1289k, Melbourne, VIC 3001, Australia.
E-mail: b.timbal@bom.gov.au

be able to explain the rainfall decline. A major research program in Australia, the Indian Ocean Climate Initiative (IOCI), was launched to study this important climate change and its causes and suggests likely future rainfall projections. More recent studies using general circulation models (GCMs; Smith et al. 2000; IOCI Panel 1999) have confirmed that SST anomalies alone cannot explain the rainfall trend, but statistical downscaling techniques (Charles et al. 1999; Timbal 2004) have been able to capture the trend accurately by relating rainfall to large-scale atmospheric changes. On the balance of the scientific evidence, the IOCI Panel (2001) has suggested that natural variability and anthropogenic climate change are the most plausible causes of the rainfall decline. Local land clearance was also identified as a plausible candidate; Pitman et al. (2004) have been able to simulate a similar but much smaller rainfall decline to that observed by reducing forest cover in a perpetual July model simulation. However, precise attribution of this regional climate change to any particular forcing remains elusive.

To attribute the forcing of the rainfall decline, the most widespread approach is to integrate a GCM using a set of forcings and compare the response of each experiment to observed changes. This study makes use of several integrations of a coupled atmospheric oceanic GCM over the twentieth century using a range of observed forcing—natural variations such as volcanoes and solar variability as well as human-induced changes in greenhouse gases, stratospheric ozone concentration, and direct sulfate aerosols (Meehl et al. 2004). Ensembles of simulations were performed to quantify the uncertainties in the model response associated with internally generated stochastic variability within the climate system and to express statistical confidence in the results. This approach is critical to attribute the cause of a regional rainfall change. Anthropogenic climate change attribution is more difficult when the meteorological variable considered exhibits large spatiotemporal variability (see Mitchell et al. 2001 for a review of attribution studies). Therefore, only a limited number of attempts have been made to attribute the cause of rainfall trend, and they tend to focus on global rainfall (Allen and Ingram 2002; Meehl et al. 2003; Gillett et al. 2004) or rainfall over large continental areas (Lambert et al. 2004). A particular issue here is the size of the area of interest compared with typical GCM grid size. Most of the winter rainfall decrease occurs within an area of 500 km by 500 km, which is covered by only four grid boxes in a typical 2.5° medium horizontal resolution GCM. Furthermore, due to heavy numerical smoothing, GCMs lack realistic features on a spatial scale smaller than several grid cells (McAvaney et al. 2001), and are likely to strongly underestimate localized rainfall maxima. For example, Smith et al. (2000) reported on a GCM forced with observed SSTs over the past century that produced an increase in total rainfall instead of the observed decline. One possible explanation raised by the authors is that "rainfall is not sufficiently well simulated by large-scale climate models to capture trends at the relatively small scale" (Smith et al. 2000, p. vii).

Regionalization techniques, either dynamical (Giorgi et al. 1990) or statistical (Hewitson and Crane 1996), have been used extensively to complement GCM simulations for small geographical scales. Statistical techniques in particular are able to reduce the problems. Timbal and McAvaney (2001) developed a statistical downscaling technique based on the analog approach first described by Lorenz (1969) for local daily temperatures. Timbal (2004) showed that the technique applied to rainfall occurrences and amounts could relate the local rainfall trend in SWA to two large-scale predictors—MSLP and the vertical integration of the moisture in the atmosphere, precipitable water (PWTR). An additional advantage of the statistical techniques is that they can be easily adapted to many different locations and have a minor computing cost. The method also allows a quantitative assessment of the uncertainties associated with the chaotic nature of the climate system and the assumed statistical relationship used (Benestad 2004).

In this article, we first describe the rainfall decline in SWA from the observations, as well as other observed regional changes in section 2. Details on the climate model simulations of the past twentieth century used here are provided and the model's ability to reproduce the large-scale changes and the local rainfall trend under several forcing are discussed in section 3. The statistical technique is adapted to the study (section 4), before results from the downscaling of the model simulations are shown in section 5. Finally, the possible attribution of the SWA rainfall decline to anthropogenic forcing is discussed in section 6.

2. Rainfall trend in the southwest of Australia and other observed relevant climate changes

The southwest tip of the Australian continent, below a line running northwest to southeast from 28°S, 115°E to 34°S, 124°E, enjoys a Mediterranean climate with a very hot dry summer and a mild wet winter. It is a small climatic entity on the edge of a large dry continent, surrounded by large ocean masses. Offshore, the warm Leeuwin Current flows southward from the Tropics along the west coast of Australia and the annual mean

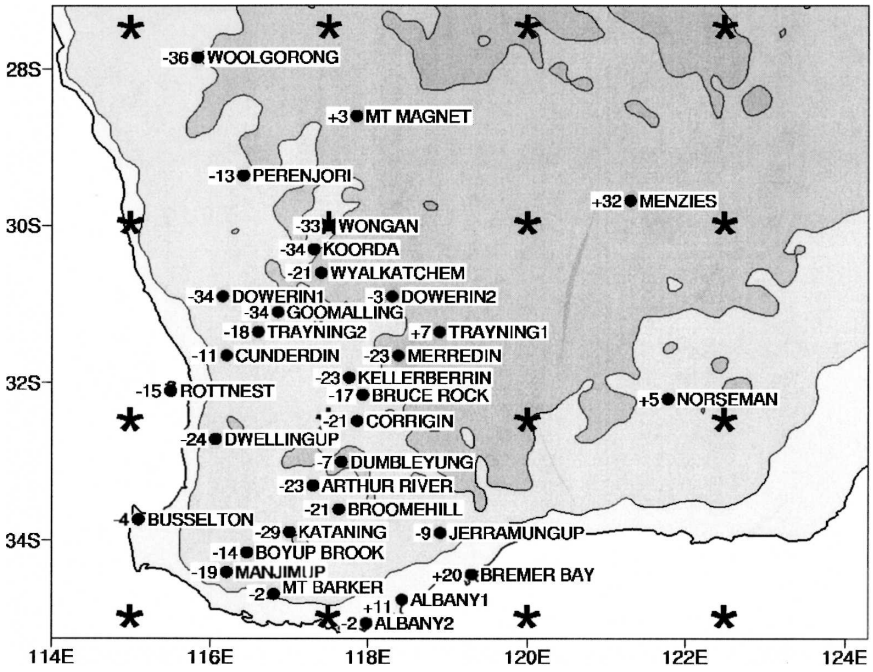

FIG. 1. High-quality rainfall stations used in SWA, and observed rainfall reduction during the 1958–98 period expressed as a linear trend in percentage of the early winter (MJJ) rainfall. The shading indicates elevation starting from sea level and with 200-m isolines. Reanalyses grid coordinates are shown as black asterisks.

SST is around 20°C offshore from Perth. Rainfall is highly seasonal with up to 80% of the rain being recorded during a 6-month period from May to October (Wright 1974a,b). The average annual rainfall is 600 mm, with local maxima on the western escarpment (such as Dwellingup, Australia) in excess of 1000 mm. It differs from other locations at similar latitude on the western edges of landmasses such as Africa or South America (which have cold coastal currents flowing toward the equator) with temperatures around 15° or 16°C and receives less than 300 mm of rainfall annually (Gentilli 1972).

Daily rainfall observations are used at 32 sites (Fig. 1). Many more rain gauges have been or are currently used in this region, but we only used sites providing high-quality daily observations over the past 45 yr, according to the analysis by Lavery et al. (1992), updated by Lavery et al. (1997). Although this criterion reduces the number of possible observations, it is mandatory, as the performances of the statistical model are strongly impacted by the quality of the predictands (Timbal et al. 2003). Most of the stations are located west of 120°E within an extensive crop-growing area known as the "wheat belt" of Western Australia. Farther east, observation density becomes low in sparsely populated areas. The reliability of the data is high and very few days are reported as missing. Over the 1958–98 period, 50% of the stations had less than 1% of missing data.

The early winter (May–July) drying trend observed in the region (expressed in percentage of the total winter rainfall) using a best linear fit for the observations from 1958 to 1998 is shown at each station (Fig. 1). A large area of strong rainfall decrease ranging from 15% to 35% affects the central and southern part of the region, with small patches of small decrease or even increased rainfall inland (farther east and north) and along the Southern Ocean coast. Most of this drying trend occurred in the 1960s and 1970s, with no significant trend in the 1980s and 1990s. In contrast, in spring (not shown), the 32-stations' average rainfall totals increase slightly (by less than 10 mm over 40 yr) without any coherent spatial pattern.

The rainfall trend is only one element of a range of climatic indices that have exhibited significant changes on a regional scale. SSTs have increased in most of the south Indian Ocean (IOCI Panel 1999, 1–52) as did MSLP around Perth (Allan and Haylock 1993). Several studies have linked the local rainfall decrease to the large-scale changes in atmospheric conditions (Allan and Haylock 1993; Charles et al. 1999; Timbal 2004).

To assess large-scale climatic change, we use the National Centers for Environmental Prediction–National

Center for Atmospheric Research (NCEP–NCAR) Reanalysis (NNR). This is a record of global analyses of atmospheric fields, on a 2.5° × 2.5° grid, from 1958 to the present (Kalnay et al. 1996). The NNR is produced using a frozen global data assimilation system. Most of the output variables used in this study are strongly influenced by observed data. For example, MSLP in the NNR exhibits a positive trend across the Australian continent with large values over SWA (this is shown in Fig. 8 and discussed later), consistent with the observation in Perth. However, some variables are strongly affected by the performance of the NNR model. Rainfall is a good example; no rainfall measurements are assimilated by the model, and Timbal (2004) showed that despite the "perfect" knowledge of the large-scale atmospheric evolution, the NNR model suggests an upward rainfall trend in SWA, contrary to what was observed. Either the model resolution (about 250-km grid spacing) or the physical scheme used to parameterize rainfall is not able to handle the particular behavior observed in this small region. In contrast, the downscaling technique bypasses the physical parameterizations to resolve the scaling issue and therefore has the ability to interpret the large-scale atmospheric forcing to reproduce the local observed trend.

3. Ensembles of simulations of the twentieth century

A large number of model simulations describing the twentieth century were performed with the Parallel Climate Model (PCM) developed by NCAR with support from the Department of Energy (Washington et al. 2000). It is based on version 3 of the Community Climate Model (CCM), described in Kiehl et al. (1998). The spectral atmospheric model has a wavenumber truncation of T42 giving an approximate grid resolution of 280 km by 280 km. The atmosphere is coupled to the NCAR land surface model (Bonan 1996), the Parallel Ocean Program (POP), with 32 vertical layers, roughly two-thirds of a degree in horizontal resolution down to one-half of a degree around the equator, and a dynamic and viscous plastic ice rheology (Zhang and Hibler 1997). The model, despite not being flux corrected, exhibits a drift of only 0.03°C century^{-1} over 1000-yr-long integrations (Meehl et al. 2004).

In this study, we use two ensembles of four experiments. After spin up to 1870 conditions, the four experiments, each starting from a different initial state at least 10 yr apart in the control run, are integrated with time-evolving forcing from 1870 to 1999. Meehl et al. (2004) provide a comprehensive description of the experimental framework and the various forcing datasets (see references therein). The first ensemble, natural (Nat), is forced by solar input variability and stratospheric sulfate aerosols from major volcanic eruptions. In the second ensemble, three anthropogenic forcings (greenhouse gases, sulfate aerosols, and stratospheric ozone) are combined with the natural forcing to produce the full-forcing (FF) ensemble. The global model response to individual and combinations of these forcings was documented by Santer et al. (2003) and Meehl et al. (2004); only results relevant to this study are mentioned here.

The global temperature responses for both the FF and Nat ensembles were compared with the globally averaged observed temperature (Folland et al. 2001) for the entire twentieth century (see Fig. 2d of Meehl et al. 2004 and relevant discussion). From the late-1960s onward, the Nat ensemble, despite strong interannual and decadal variability, does not match the observed variability, while the FF ensemble does. This suggests that the observed global warming in the second half of the century cannot be explained by natural causes.

Here, we will examine large-scale climate variables in and around SWA and compare them to observed values. For example, Fig. 2a indicates how well the model has captured the observed variability over the southern Indian Ocean in the Nat and FF ensembles. The black solid line depicts the observational estimate of sea surface temperature averaged over the southern Indian Ocean using the southern Indian Ocean index (SIOI) from 35° to 45°S and from 10° to 150°E with its mean value removed. The index was calculated using the United Kingdom Met Office (UKMO) SST dataset (Rayner et al. 2003). The plot shows a 20-yr running average of the SIOI. The mean and model mean were removed from the observation and from both ensembles, respectively.

The gray lines represent the 95% confidence interval for the same index in the Nat ensemble. This range is due to the differences that can arise between the different Nat runs because of the partially chaotic nature of the climate system, that is, due to internally generated variability. The confidence intervals were estimated using $\mu \pm 1.96[1 + (1/\sqrt{N})]\sigma$, where μ is the ensemble mean of the 20-yr running average of SIOI in the Nat ensemble, σ is the estimated standard deviation of the scatter among ensemble members in the Nat ensemble, and N is the number of simulations per ensemble (i.e., four). Here, σ is estimated from the variability of the 20-yr averages in all of the runs considered (not just the "Nat" simulations), about their corresponding ensemble means, described by Meehl et al.

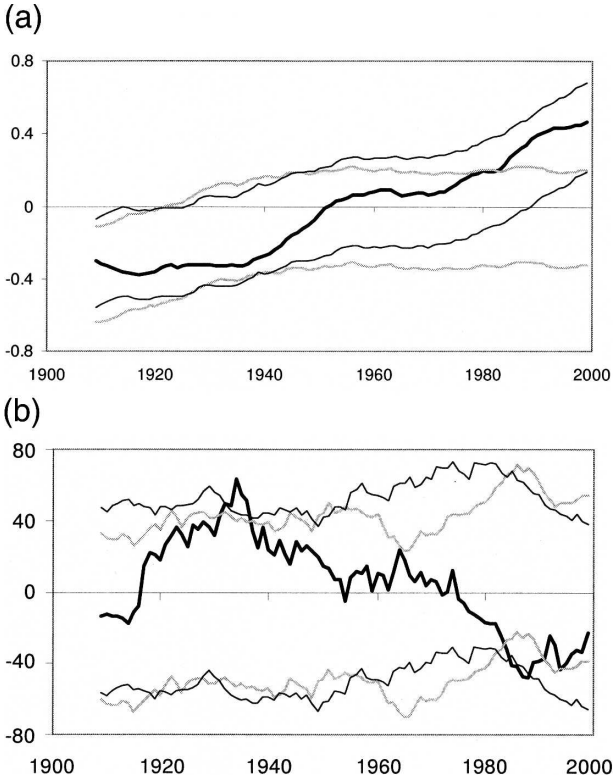

FIG. 2. (top) The 20-yr running average observed SST anomalies in the southern Indian Ocean (black thick line), full forcing (thin black line), and natural forcing (gray line) ensemble estimates at the 95% confidence level. (bottom) Same as (top) but for rainfall in SWA.

(2004). The thin black lines give the 95% confidence interval for the 20-yr running average of the SIOI in the FF ensemble. Notice that the long-term trend in the observed SIOI falls within the 95% confidence interval for the FF run, whereas it is beyond the Nat interval for the last 20 yr. The long-term trend evident in SIOI is therefore better captured in the FF ensemble, that is, in the run in which anthropogenic forcing is included.

A similar plot is depicted in Fig. 2b, this time for the SWA rainfall anomaly average. The gridded rainfall dataset used here (Jones and Weymouth 1997) consists of monthly averages on a regular 1° by 1° latitude–longitude grid covering the Australian continent for the period from January 1900 to December 2002 inclusive. The data were area averaged over land in the southwest (i.e., 31°–35°S, 110°–118°E) to form a simple index. Model rainfall was extracted from grid points falling within the same domain but from the model grid. The Nat and FF ensembles capture most of the observed variability; the observed rainfall in two occasions steps outside the 95% confidence interval for both runs. For the FF ensemble these two occasions do not exceed 5% of the time and therefore could have been obtained by chance. Not so for the Nat ensemble, but the difference between the two ensembles is very small. The most interesting feature in the plot is of course the major drying that has been observed since the mid-1960s. The FF ensemble also simulates drying toward the end of the run but a similar amount of drying is evident earlier in the century in the Nat ensemble. This indicates that the model can produce sustained drying events without anthropogenic forcing. The trends in SWA from the two ensembles suggest that while surface warming in the region is probably anthropogenically forced, the drying might very well be a natural event, though there is a hint that anthropogenic forcing might increase the risk of drying.

This reinforces the fact that regional rainfall is a difficult quantity to simulate, as found in other studies (Gillett et al. 2004) and stated earlier. Models are much better at simulating large-scale changes in the atmosphere and ocean. In fact, models tend to be better at simulating large-scale changes linked to rainfall variability than they are at simulating the rainfall variability itself, as was mentioned earlier for the NNR. An example of the deficiencies of rainfall characteristics on a regional scale is given in Table 1. The percentages of observed rainfall, reproduced by both ensembles over the six grid boxes covering SWA, are shown for total rainfall amounts and rainfall occurrences in winter and spring. Despite a large (to very large in the winter) overestimation of rainfall occurrences, rainfall amounts are underestimated in both seasons.

These large biases in the mean climatic state cast doubt on the ability of the model, even with a realistic forcing, to reproduce local rainfall variability. Using a downscaling technique to correct model biases and to exploit the ability of the model to simulate large-scale features will provide a more realistic framework to examine long-term trends in large-scale atmospheric fields and link it to rainfall changes in SWA. In turn, this methodology will provide a better way to deter-

TABLE 1. Direct model SWA rainfall, total amount, and rain days, for each ensemble mean as a percentage of the observations for both (top) winter and (bottom) spring.

Winter rainfall	Obs	Natural	FF
Mean	205 mm	80%	82%
Occurrence	39 days	140%	142%
Spring rainfall	**Obs**	**Natural**	**FF**
Mean	129 mm	60%	58%
Occurrence	31 days	113%	111%

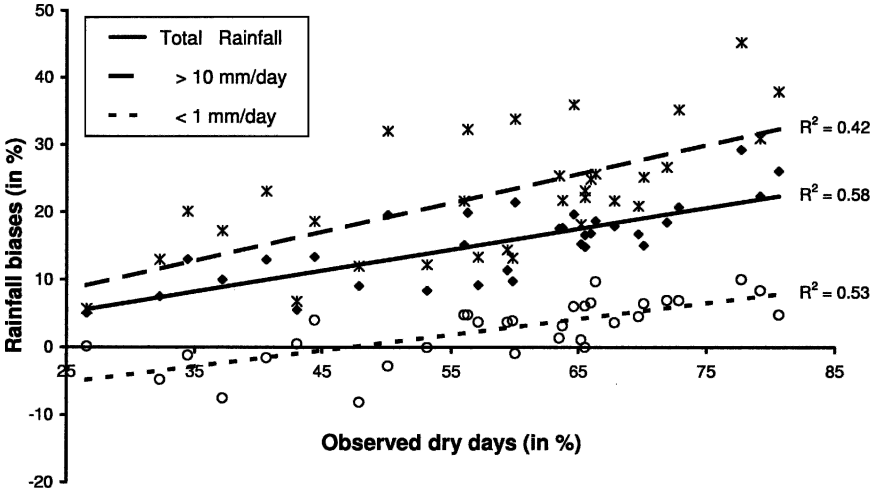

FIG. 3. Rainfall biases as a percentage of the total amount as a function of the number of dry days (in %), for total (black diamonds), heavy (stars), and light rainfall (open circles). For each category, a linear trend is fitted on the data and the percentage of explained variance is given.

mine the extent to which the recent drying can be attributed to anthropogenic and/or natural forcing.

4. Evaluation of the downscaling technique using the reanalyses

Timbal (2004) adapted a statistical model (SM) based on an analog approach and developed earlier for daily maximum temperature (Timbal and McAvaney 2001) to downscale large-scale atmospheric fields to local observed rainfall in SWA. The technique, applied to the NNR, was shown to be successful in reproducing the observed rainfall trend in the second half of the twentieth century. The result demonstrates the benefit of using a statistical downscaling approach to complement GCM results since the NNR direct model rainfall exhibits the opposite trend to what has been observed. However, there are two limitations in applying the technique, as described in Timbal (2004), directly to the PCM ensembles: 1) the reconstructed series underestimated the observed variance that impacted the reproduction of the rainfall trend; and 2) daily PWTR is not available from PCM ensembles and therefore other moisture predictors available at daily time steps from PCM simulations must be tested. We shall now look at ways to improve and adapt the technique for the downscaling of the PCM ensembles.

A common limitation of statistical downscaling techniques is that they underestimate the observed variance of the reconstructed rainfall. Although the analog approach is less affected than other techniques (see Imbert and Benestad 2005 for a recent comparison), Timbal (2004) reported that the analog reconstructed series for SWA rainfall underestimated the observed variance by up to 30%. It was further shown that this underestimation gives rise to a dry bias in the reconstructed series, due to the highly skewed distribution of daily rainfall.

Simple inflation methods have been developed to reproduce the observed variance, but these rely on the false assumption that local variability is entirely driven by large-scale variability (von Storch 1999). In the case of the analog approach, it has been shown that the quality of the model depends on, among other factors, the size of the sample available to search for an analog (Van den Dool 1989; Timbal et al. 2003). A hypothesis to explain the reduced variance is that the extreme rainfall events are difficult to reproduce because of the limited size of the pool of analog situations. If true, one would expect that the variance reduction would be dependent on the percentage of observed rain days and should affect larger rainfall events.

There is a strong positive relation between the dry bias and the percentage of dry days (Fig. 3). This suggests that the smaller the pool of rainfall occurrences from which to choose a similar wet day, the more likely it is that the analog model will pick a dry day. This will lead to an underestimation of both the total rainfall and daily variability. Averaged over the 32 stations, observed light rainfall (<1 mm day^{-1}) occurs 27.5% of the time while medium (between 1 and 10 mm day^{-1}) and heavy (>10 mm day^{-1}) rainfall occurs on average 7.2% and 6.9% of the time, respectively, but these numbers vary greatly from the wettest to the driest stations; rain-

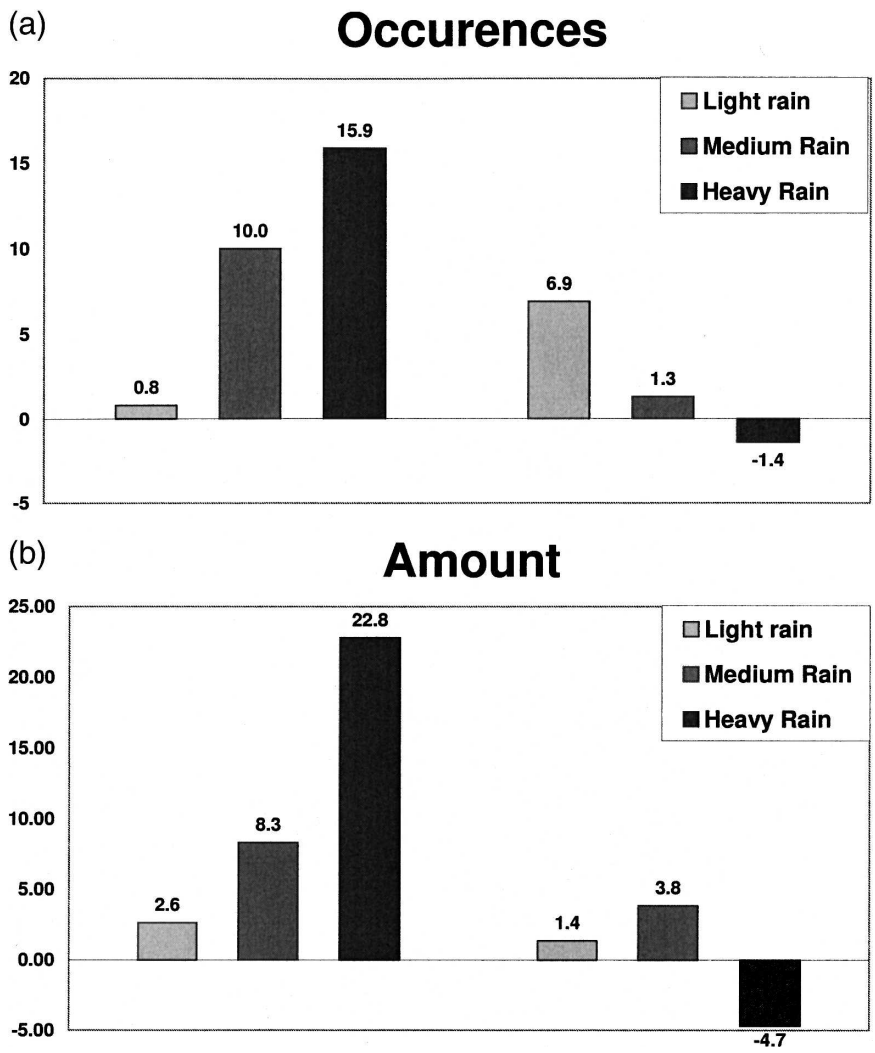

FIG. 4. (a) Rainfall biases for light, medium, and heavy rainfall occurrences expressed in percentage of the total value, (left) without and (right) with a correction factor. (b) Same as (a) but for amount.

fall occurrences range from 25% to 80%. A split between light, medium, and heavy rainfall shows that the largest biases are observed for heavier rainfall categories. Heavy rainfall days are the least frequent events. The slope of the positive relationship increases with the intensity of the rainfall events. Heavy rainfall occurrences can be as low as 2.5% of the time for the driest locations, reducing the pool of analogs by a factor of 40, producing biases in excess of 30%. These results are consistent with the hypothesis that the analog-reconstructed rainfall is impacted by the size of the pool of analogs to choose from and this leads to larger errors in the more extreme cases. Therefore, an attempt is made to correct reconstructed rainfall series based on the observed rainfall occurrences, applying the following correction factor to multiply rainfall observed on any analog day:

$$C_{\text{factor}} = 1 + 0.1 \times \frac{N_{\text{dry}}}{N_{\text{wet}}} \quad \text{with an upper limit of 1.5,} \tag{1}$$

where N_{dry} and N_{wet} are the numbers of dry and wet (>0.3 mm) days observed for the season at each individual location, respectively.

The impact of the correction factor on the reconstructed series of rainfall occurrences and amounts is shown in Fig. 4. The biases for all three categories, in percentage of the observed rainfall, have been reduced with the introduction of the correction factor in all

TABLE 2. Impact of the correction factor on total rainfall amount and daily variance in (top) winter and (bottom) spring.

Winter bias	Without correction	With correction
Mean	−17.5%	−0.8%
Variance	−31.5%	+1.5%
Spring bias	Without correction	With correction
Mean	−26.1%	−2.5%
Variance	−41.6%	+2.0%

cases except for light rainfall occurrences. The reduction is larger for the heavy rainfall events where the bias is the largest.

The aggregation of all rainfall categories eliminates the net bias for rainfall total amount and rainfall daily variance observed in Timbal (2004). The mean rainfall bias was reduced from 17.5% to less than 1%, and the variance bias has been reduced from 31.5% to a slight overestimation of 1.5% (Table 2). The same correction factor [Eq. (1)] was applied to spring rainfall and yielded similar results for rainfall categories. The bias in total rainfall amount has been reduced from 26.1% to 2.5% and the variance bias from 41.6% to an overestimation of 2%. The robustness (across stations and seasons) and simplicity of the correction factor makes it an effective way to eliminate the variance underestimation and therefore the dry bias of the reconstructed rainfall series.

We shall now turn to the analysis of the performance of the moisture fields available from PCM. The performance of PWTR (used in Timbal 2004) was compared with moisture variables available as daily outputs from the PCM ensembles: large-scale convective and total rainfall. Each moisture predictor was tested as a sole predictor and in combination with MSLP; results are compared in Table 3. A range of statistics for rainfall amounts and occurrences are averaged over the 32 stations. Total rainfall occurrences, mean rainfall amounts, and daily variability, given as a percentage of the observed values, are used to assess the overall properties of the reconstructed series. The skill of the analog model to reproduce day-to-day rainfall was compared with the NNR direct model output (DMO) rainfall. The statistics used are the daily correlation for rainfall amount and the following index for rainfall occurrence:

$$I = 100 \times \left(1 - \frac{m}{w+m} - \frac{f}{d+f}\right), \qquad (2)$$

where w is a wet day (more than 0.1 mm day^{-1}) reconstructed and observed, d is a dry day (less than 0.1 mm day^{-1}) reconstructed and observed, m is a wet day missed by the forecast, and f is a dry day falsely forecast as wet.

This index gives 100% for a perfect forecast ($m = f = 0$). It would give a value of 0 for a random choice of uncorrelated days ($w = m$ and $f = d$). This index also takes into account the asymmetrical partition between dry and wet days. A simple scheme of extreme persistence, which would assume either rain (or no rain) every day, would have a score of 0 unless such extreme persistence is true to the observation, giving a perfect score of 100%.

Finally, the reproduction of the observed drying trend expressed in millimeters per year was also compared to the observed value.

Each statistical model was slightly perturbed to sample the robustness of each of the statistics used to assess the SM performance. The parameter that was allowed to vary is the number of calendar days that can separate the date of the analog from the original date (D_{tcal}); values of 15, 20, 30, and 60 days were used. As an example, when D_{tcal} is set to 15 days, an analog for 15 June 1996 can be found in any calendar year but only between 1 and 30 June. Table 3 results are expressed in

TABLE 3. Statistics of the 32-station average of the reconstructed series using a range of predictors, compared with observation: total rainfall occurrence, a skill score of rain occurrence, total rainfall amount, daily variances, daily correlation, and the trend over the 1958–98 period. Total occurrence and amounts as well as variance are expressed in percentage of the observed values; daily correlation and occurrence indices are direct measures of the skill of the predictors and have no units; trends are in mm yr^{-1}. Uncertainties are assessed using four SMs.

Predictors	Rain occurrence	Occurrence index	Total amount	Daily variances	Daily correlation	Slope (Obs: −0.69)
MSLP	94.7–95.4	38.4–39.3	101–103	107–111	0.31–0.32	−0.35 −0.55
PWTR	96.2–97.9	29.8–31.0	102–107	107–113	0.24–0.25	−1.04 −1.56
Total rainfall	90.1–91.7	31.9–32.9	91–94	91–95	0.32–0.33	+0.77 +1.19
LS rainfall	89.5–91.3	20.2–21.3	95–100	104–109	0.21–0.22	−0.48 −0.61
MSLP and PWTR	92.8–94.2	39.7–40.5	95–100	97–105	0.35–0.37	−0.70 −1.07
MSLP and total rainfall	92.4–93.5	38.9–39.8	95–97	96–99	0.36–0.37	−0.03 +0.27
MSLP and LS rainfall	93.6–94.3	37.9–38.6	98–100	101–102	0.32–0.34	−0.24 −0.85
NNR DMO rainfall	77.3	29.9	64	39	0.25	0.79

range; this parameter helps determine robust statistics (such as daily correlation of rainfall amount and occurrence index for which ranges are very small) from more uncertain statistics such as the reproduction of the drying trend.

Among single predictors, MSLP is the best predictor across the range of statistics used but in particular for rain occurrence. PWTR gave the smallest bias for total rain occurrences; large-scale rainfall gave the best estimate for total rainfall amount and daily variability; total rainfall gave the best correlation with observed rainfall amount. It is interesting to note that while total rainfall leads to a positive trend for rainfall over the 1958–98 period consistent with the NNR DMO, large-scale rainfall alone gives a drying trend consistent with what was observed. This result provides some explanation on why NNR DMO rainfall has a trend toward a wetter climate in SWA contrary to the observation. Large-scale rainfall only accounts for less than 20% of the total rainfall in winter, which is far less than the 55% or more suggested by the Tropical Rainfall Measuring Mission (TRMM) satellite measurement outside the Tropics in the Southern Hemisphere (Schumacher and Houze 2003). Commonwealth Bureau of Meteorology forecasters from the Western Australia office, who routinely observed rainfall patterns in this region, estimate that between 25% and 70% of the rainfall, depending on the location, is large scale (N. Puzey and G. Cook 2005, personal communication). Therefore, it is plausible to relate the positive trend in the total rainfall to the wrong partition between large-scale and convective rainfalls within the model and to the competing trends between decreasing large-scale and increasing convective rainfalls. While plausible, testing this hypothesis would require a study beyond the scope of this article.

Outside the combination of MSLP and PWTR, MSLP with large-scale rainfall gave the best result for rainfall occurrences, total amount and daily variability, although skill scores such as the occurrence index and the daily correction for rainfall amount are higher with MSLP combined with total rainfall. At face value, both rainfalls look like they are of equal value, however the focus of this study is to reproduce the observed rainfall decline during the second half on the century. For this reason, the combination of MSLP and total rainfall that produces increasing rainfall during the period, due to the total rainfall contribution, is not suitable. On the other hand, the combination of MSLP and large-scale rainfall uses two predictors that both contribute to the explanation of the observed rainfall decline and therefore are more likely to translate large-scale changes, if the model ensembles are consistent with the reanalyses into local rainfall decline as observed.

Therefore, the chosen SM for the rest of the study combines MSLP and large-scale rainfall as predictors. As expected, the SM gives better results all around than direct rainfall as modeled by the NNR, using the nearest grid point for each station (last row in Table 3). The differences outline the benefit of the downscaling technique in reducing GCM biases.

It is expected that the SM would reproduce the geographical pattern of the SWA rainfall decline. The observed rainfall decline, expressed in millimeters per year (Fig. 5a), exhibits some coherent spatial features. The largest absolute values are observed alongside the escarpment near the west coast of SWA. Values typically exceed 1 mm yr^{-1} and are up to 3.8 mm yr^{-1}. Inland, values tend to be lower. Coastal locations near the south coast show a lot of spatial variability but overall have lower drying trends and in some cases exhibit positive trends. More remote inland stations also show positive rainfall trends. The overall pattern is realistically reproduced by the reconstructed series based on the combination of MSLP and large-scale (LS) rainfall (Fig. 5b) with the largest drying trends near the west coast and smaller trends inland. Trends are positive along the entire south coast. The observed contrast between west and east is not as pronounced in the analog reconstructed series. The reconstructed rainfall series using only LS rainfall as a predictor (Fig. 5d) shows a relatively uniform drying trend with a pattern that does not match the observations. In contrast, the reconstructed series using MSLP as a predictor (Fig. 5c) shows a slightly smaller trend but a more realistic geographical pattern. These results confirm earlier findings that the overall drying trend is best explained using both MSLP and a moisture field (Charles et al. 1999) and that MSLP is particularly important to explain the geographical distribution of the trends while the moisture field is a key component of the intensity of the rainfall reduction (Timbal 2004).

5. Downscaling of the PCM ensembles

In the previous section, the statistical model was adapted to this study and optimized to reproduce the rainfall decline. Here we will apply exactly the same SM to both sets of ensembles. Daily hindcasts from 1958 to 1998 were matched with a reanalysis from the same period. To search for the best analog, anomalies of the large-scale predictors (MSLP and large-scale rainfall) from the 41-yr winter mean were used and normalized separately for each individual simulation and the NNR. Rainfall series were reconstructed over the 41 yr at

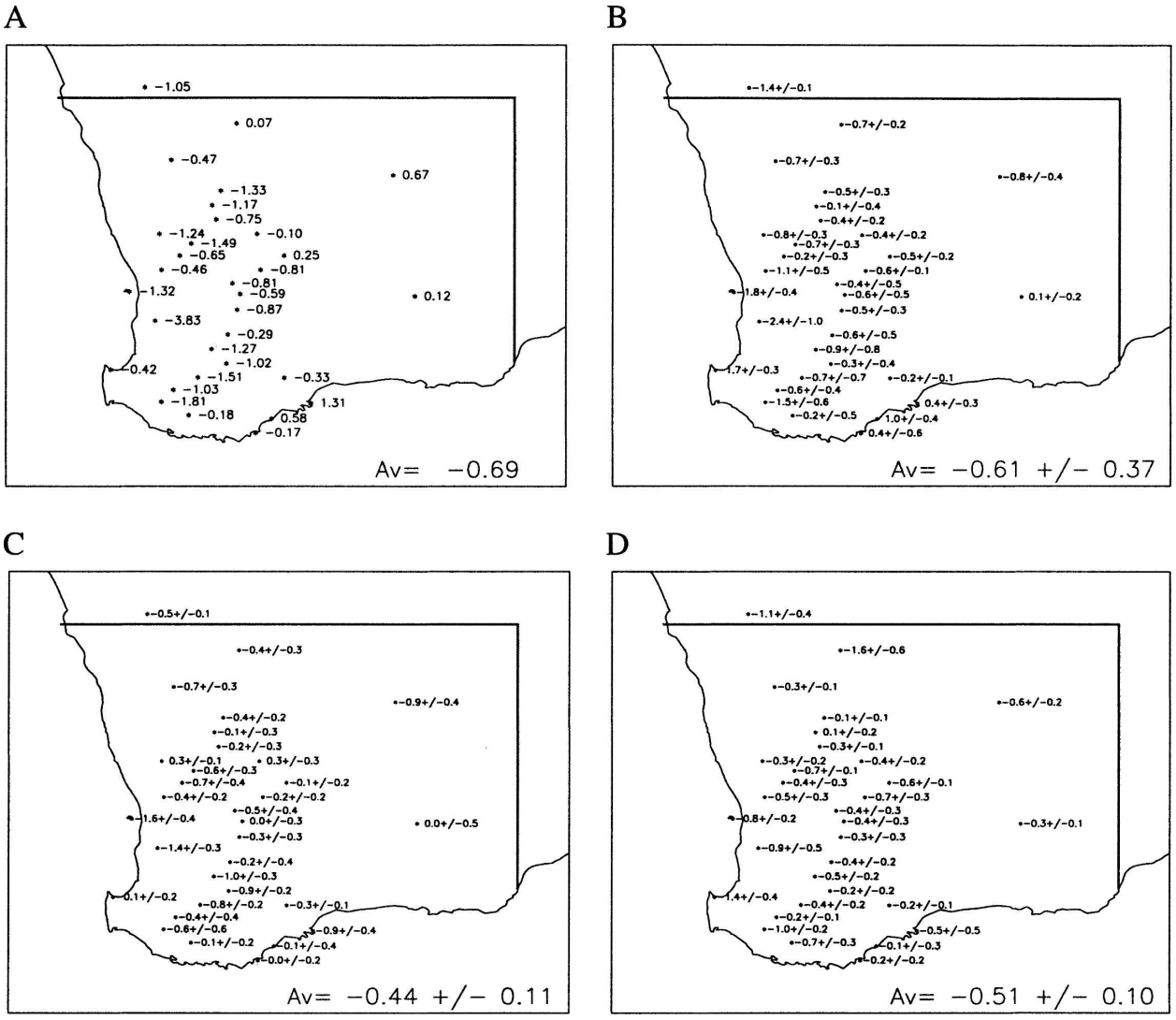

FIG. 5. Station-by-station winter rainfall decline expressed as a linear trend in mm yr^{-1} for (a) observed series, (b) SM-reconstructed series, with uncertainties attached, using MSLP and LS rainfall as predictors, (c) using MSLP alone, and (d) using LS rainfall alone.

each station and compared with observations. Uncertainties related to the downscaling method were identified using perturbation of the SM. The parameter that was allowed to vary is the number of calendar days that can separate the date of the analog from the original date (D_{tcal}); values of 15, 20, 30, and 60 days were used as per the technique development part. Global statistics such as the total rainfall, daily variance, and rainfall occurrences were in line with what was expected. Biases in both the Nat and FF ensembles are very similar.

Linear trends were fitted for each reconstructed series and averaged over the 32 stations (Figs. 6a,b). Individual stations exhibit large ranges, typically about ± 1 mm yr^{-1} and up to 3 mm yr^{-1}. This range is due to the internally generated variability and uncertainties arising from the statistical linkage. The 32-station average range is also large and overlaps between the two ensembles. But only the mean of the FF ensemble suggests a drying trend, albeit about half of the observed value, with a range of uncertainties encompassing the observed value (-0.69 mm yr^{-1}), while the Nat ensemble mean is positive and the observed value is outside the possible range from this ensemble. There is no requirement for the mean of the ensemble to match the observed trend, which is only one realization of the chaotic climate system. The most important argument here is that the observed trend is within the downscaled FF ensemble range and outside the Nat ensemble range. Only the geographical pattern in FF (Fig. 6a) bears some resemblance to what was observed

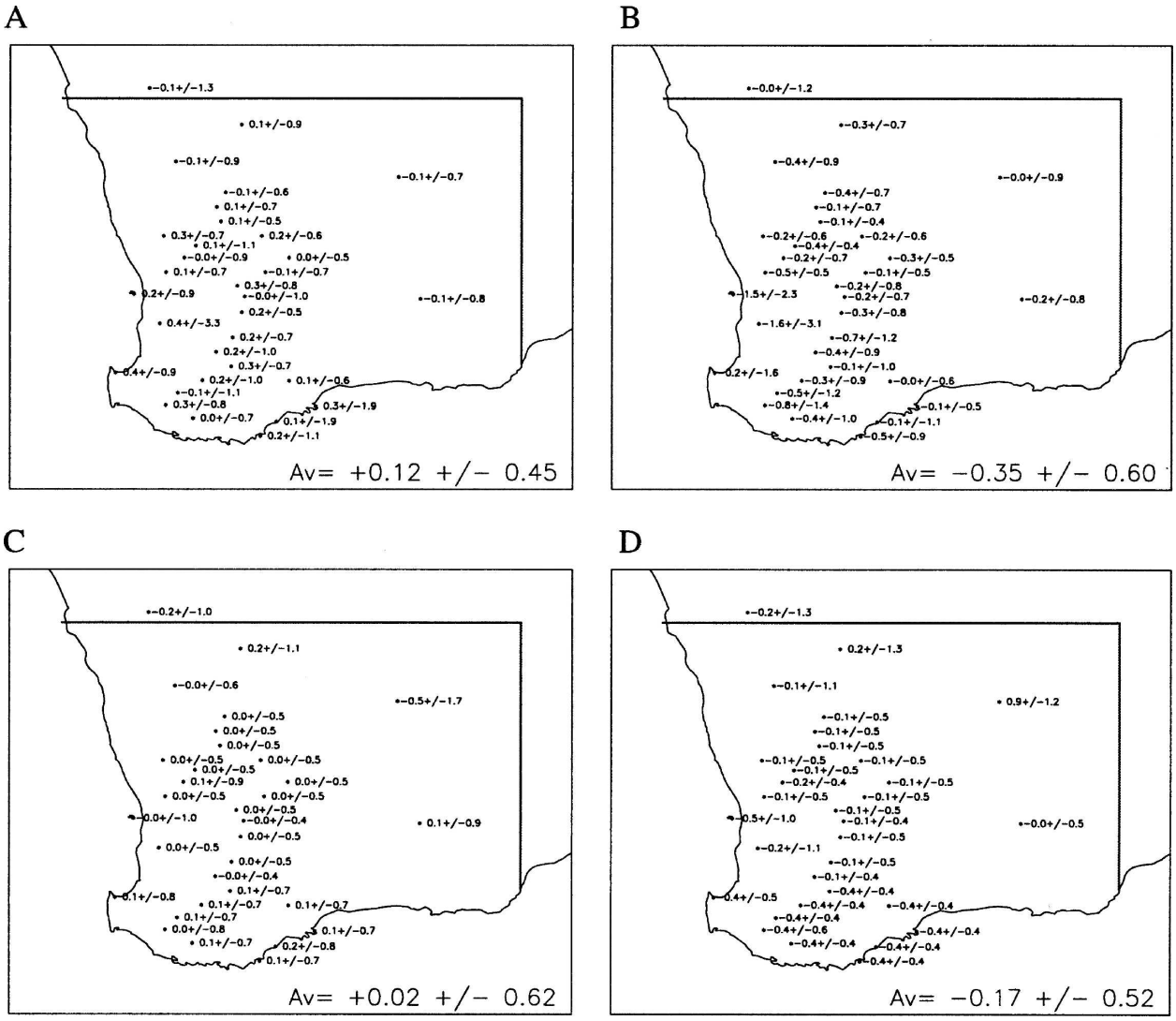

FIG. 6. Same as in Fig. 5, but for the downscaling of the (a) Nat and (b) FF. (c), (d) Same as in (a), (b) but for DMO.

(Fig. 5a). Larger values are evident in the southwestern part of the region with smaller values farther north and east. In the Nat ensemble, however, no consistent spatial patterns are apparent. Despite the overall positive trend, about a third of the stations scattered across the domain show a decreasing trend. Arguably, very few are located where the strongest rainfall decline was detected. Overall, the downscaling of the FF ensemble is more consistent with the observed rainfall decline than the Nat ensemble but the magnitude is smaller and the gradient between the southwest and northeast stations is less pronounced. Since we know from the previous section that the statistical technique does not perfectly reproduce the observed rainfall trend, it is interesting to compare the downscaling of both ensembles with the reconstructed trend based on the same predictors from the NNR (Fig. 5b). Indeed, the downscaling of the NNR and the PCM FF ensemble shows a striking resemblance. Finally, comparison with the DMO rainfall trends (Figs. 6c,d) shows that the average tendencies are consistent between downscaled and DMO rainfall. However, the separation between the two ensembles is smaller with DMO than directly to the PCM ensembles: once the downscaling is applied. In the former case, the overlap is large between the two ensembles. Furthermore, the geographical pattern shown by the FF ensemble is rather uniform and does not resemble the observed pattern.

One possible explanation for the smaller rainfall decline is the reduced interannual variability generally associated with model rainfall (McAvaney et al. 2001). The interannual range for May–July (MJJ) rainfall,

TABLE 4. Interannual range for MJJ rainfall over the 1958–98 period (in mm).

Interannual range	Obs	Down	DMO
Observation	216		
Nat		173	198
FF		161	196

over the 1958–98 period, is shown in Table 4 averaged across the four members. Both ensembles reproduce about 90% of the interannual range. The underestimation of the interannual range is rather small with DMO and larger (about 20%) with the downscaling technique. Therefore, the fact that the rainfall decline cannot be explained by the DMO rainfall in both ensembles cannot be due to the reduced rainfall internal variability in the models. The reduced interannual variability is more likely to be a factor, albeit a small one, in the downscaled reconstructed series, contributing to an underestimation of the rainfall trend.

The 32-station average based on the downscaling approach are compared with the same average based on direct model rainfall from both ensembles (Table 5). To achieve a meaningful comparison, the spatial average is a simple arithmetic mean without weighting for both DMO and downscaled values; DMO are calculated for each station using the nearest grid average as the point value. DMO and downscaled results are consistent, but in the case of DMO, the separation between the two ensemble means is more than halved and the ranges of responses from the ensemble members overlap almost completely. In contrast, the downscaling of individual members shows only one simulation within the FF ensemble, which falls within the Nat ensemble. These results indicate that although anthropogenic forcing is needed to explain the rainfall decline in SWA, the observed rainfall decline with such forcing was not a certainty as only three out of four simulations tend in this direction.

TABLE 5. Linear drying trend from 1958 to 1998, averaged over the station network in SWA, obtained from each ensemble member as DMO or using the downscaling technique, using four SMs. The ensemble mean is calculated over the four members of each ensemble.

Expt		Downscaled				DMO
	Expt 1	0.02	0.11	0.14	0.37	0.35
Natural	Expt 2	0.46	0.46	0.57	0.20	0.49
Forcing	Expt 3	−0.01	−0.05	0.12	0.20	−0.61
	Expt 4	−0.18	−0.26	−0.26	−0.17	−0.14
Ensemble	Mean			0.12		0.02
	Expt 1	−0.51	−0.42	−0.52	−0.47	−0.24
Full	Expt 2	0.08	0.12	0.05	0.25	0.35
Forcing	Expt 3	−0.38	−0.42	−0.23	−0.42	−0.64
	Expt 4	−0.95	−0.76	−0.59	−0.50	−0.16
Ensemble	Mean			−0.35		−0.17

Table 5 demonstrates that the largest contribution to the overall uncertainty in the rainfall trends comes from the internally generated variability of the climate model. Uncertainty from the statistical linkage between the large-scale predictors and the local rainfall is secondary. It is also worth noting that from each ensemble, there is at least one member for which DMO rainfall suggests a trend similar to that observed. At face value, this suggests that the model is capable of reproducing the observed trend with or without the anthropogenic forcing. However, DMO rainfall poorly captures observed rainfall in SWA, as shown earlier, and this result should be looked at carefully. Indeed, despite the overall consistency between DMO and downscaled rainfall trends, this experiment (member three of the Nat ensemble) shows near-observed rainfall decline when DMO rainfall is considered but the large-scale changes are not consistent; once downscaled, this simulation exhibits a small nonsignificant increase.

The matching of station-by-station results with observed values was further assessed for each member of the FF ensemble (Fig. 7). The graphs illustrate the range of responses from the ensemble members. Spatial correlation for the three members where the rainfall is declining ranges between 0.5 and 0.6. This correlation, across the Nat ensemble, is −0.06 (not shown). These results indicate that once the large-scale changes are consistent with what the reanalyses suggest, the local rainfall trends are consistent with the observed rainfall decline. This is the case in three out of four simulations with anthropogenic forcing added to the natural forcing.

The trends on the analog-reconstructed series are driven by the trends in the predictors. The map of the linear trends fitted to the NNR MSLP and large-scale rainfall is shown in Fig. 8 and compared with the trend from both ensemble means. The NNR exhibits a large area of increased MSLP over Australia and negative values farther south. These trends correspond to an enhancement of the high pressure belt centered on 35°S and to a shift poleward of the storm track. This trend is consistent with future projections following greenhouse gas increase (Cubasch et al. 2001) and observed changes (Gillett et al. 2003). The MSLP increase is very large in the domain used for the analog model (shown with a black box). MSLP trends are different for both ensembles. The Nat ensemble suggests a west–east contrast with a pressure decrease over SWA. The FF ensemble shows an increase of MSLP around 50°S. It is worth noting that the FF ensemble map is quite different from the NNR one but is consistent with a shift

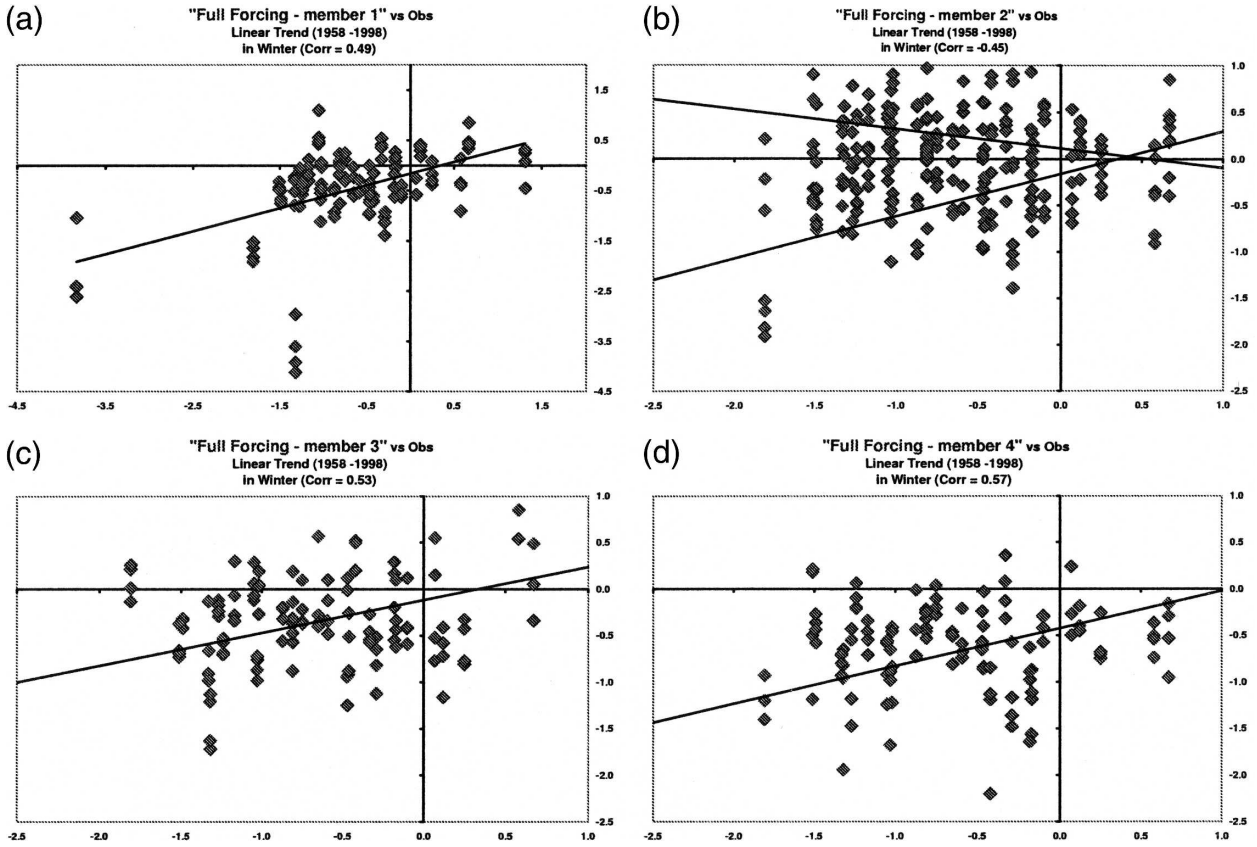

FIG. 7. Correlation between observed and reconstructed linear trends at individual stations. Series are constructed using four downscaling models for each of the four members of the FF.

poleward of the high pressure belt. The NNR also suggests a strengthening of the high pressure but farther north above the Australian continent. Similarly, a map of trends was calculated for large-scale rainfall. Both PCM ensembles exhibit smaller linear trends than the NNR. Over the Australian continent, the FF ensemble patterns more closely match the reanalyses; not so at high latitude. The differences between the two ensembles are small above the SWA region and therefore it is expected that most of the differences between the simulations are related to the MSLP changes.

A particular feature of the rainfall decline in SWA is that it occurs as a "jump" during the 1960s and 1970s (IOCI Panel 1999). Therefore, it is interesting to compare the 32-station average from observations (using a 5-yr running mean) with an estimate from the downscaling of the FF ensemble (Fig. 9). It is worth noting that the estimate of observed rainfall differs from the earlier Fig. 2 that spans a longer period and is based on gridded data using only a subset of the 32 stations. The estimate is based on the largest and smallest values given by the downscaling with the four SMs of the four members of the FF ensemble. Linear trends fitted on the observations for the two halves of the period underline the shift between the two periods. In contrast, the FF trend is well matched by a linear trend fitted on the mean of the FF estimate over the entire period. The occurrences of the drying trend in the early part of the period cannot be explained by the external forcing (natural or anthropogenic) used in the FF ensemble. Outside model or forcing deficiencies, two hypotheses can be formulated to explain this feature: 1) it is a random process due to the natural variability inherent to the climate system at time scales from decadal to interannual, and 2) it is due to other external forcing not included in these experiments, such as land clearance, which occurred mostly during the two decades when the rainfall decline occurred.

6. Discussion and final remarks

The southwest corner of Australia has experienced a very significant rainfall decline. Early winter (May–July) rainfall has decreased by about 20% since the late 1970s. Attribution of this large decrease has been attempted in this study. It is, however, a difficult task for

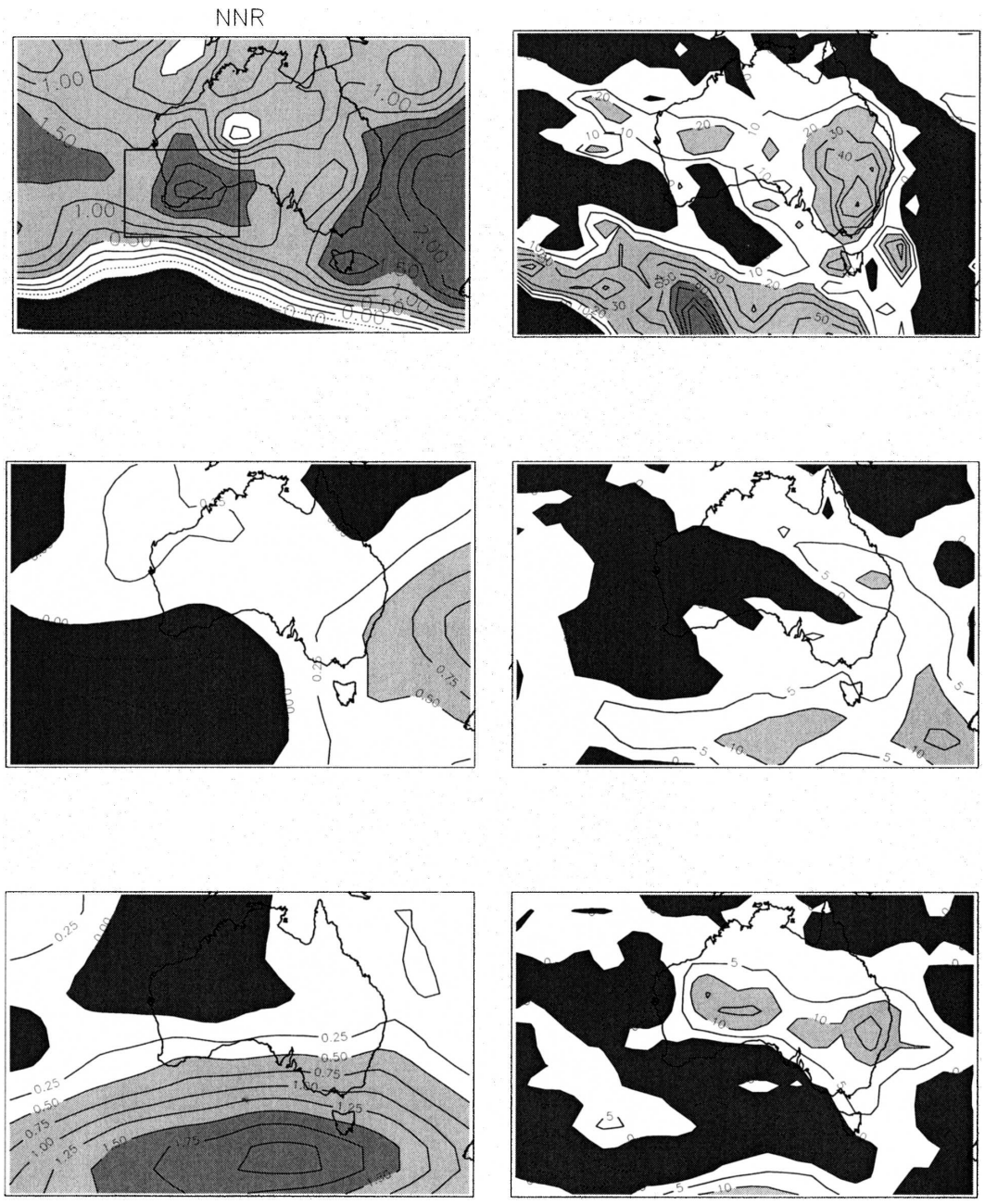

FIG. 8. Geographical maps of linear trends for (left) MSLP (hPa) and (right) LS rainfall (in mm) fitted from 1958 to 1998 for the (top) NNR, (middle) Nat, and (bottom) FF ensemble. The black box on the first map indicates the area considered within the SM.

a global climate model to simulate rainfall over such a small region, and rainfall predicted by the coupled climate model does not reproduce the characteristics of the local rainfall.

While the model reproduces planetary climate changes, it does not consistently reproduce the rainfall decline in SWA, although the spread of both ensembles is nearly large enough to encompass the observed rainfall decline. Large-scale responses of both ensembles were compared to a set of observed climate changes (global land surface temperature and south Indian Ocean SST). When the model is only forced by naturally occurring external forcing (solar variability and major volcanic eruptions), it failed to reproduce the observed global land surface and south Indian Ocean warming in the latter part of the twentieth century.

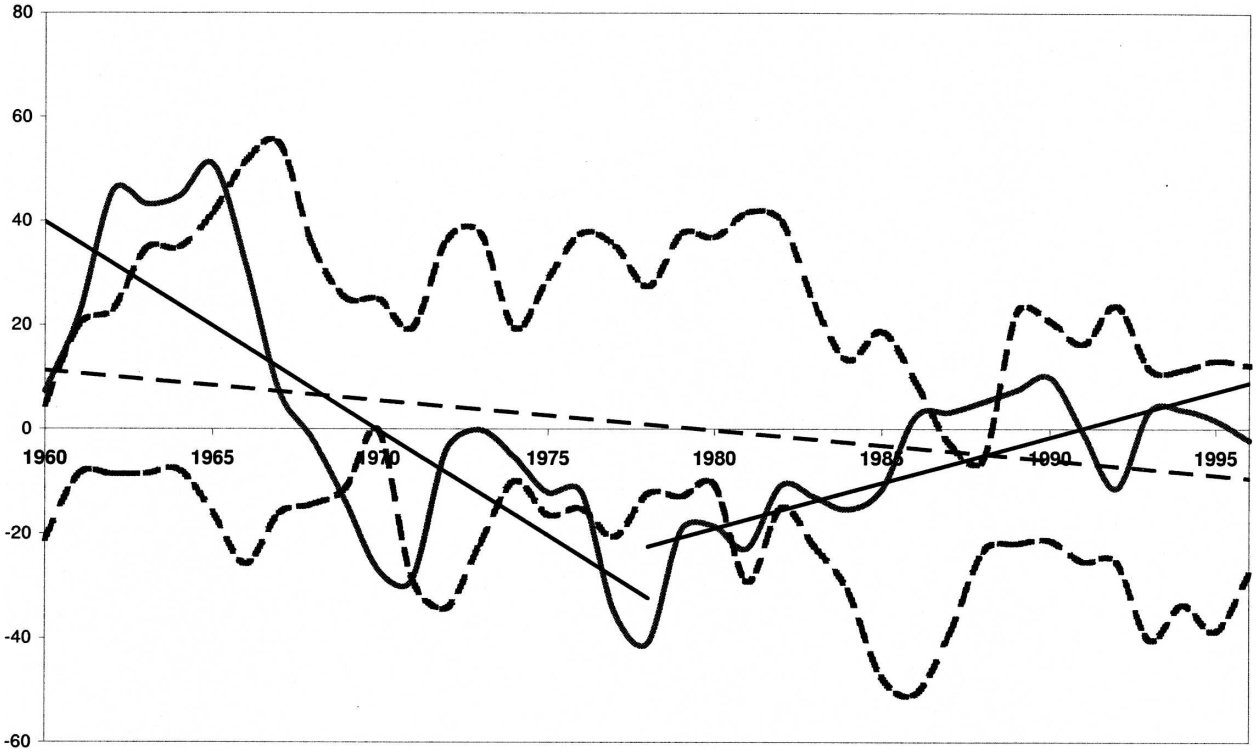

FIG. 9. The 5-yr running mean of the spatial average of SWA rainfall from 1960 to 1996 (black line) and the range from the four members of the FF (dashed lines). Linear trends have been fitted for the first and second half of the period for the observation (full line) and over the entire period for the downscaled FF ensemble (dashed line).

When the model is forced with "full forcing," that is, anthropogenic forcing (such as greenhouses gases, stratospheric ozone, and direct sulphate aerosols) as well as natural forcing, it convincingly matches the specific warming.

The ability of the FF model ensemble to produce realistic large-scale changes is exploited by adapting a downscaling technique that relies on large-scale predictors to reproduce local rainfall. The technique has been adapted to the PCM ensembles; it relies on MSLP and stratiform rainfall over a large region encompassing SWA to reproduce locally observed rainfall series. When the statistical model is applied to a "perfect" knowledge of the atmosphere provided by the NCEP–NCAR Reanalysis (NNR), it matches the observed rainfall decline. This suggests that the drying is closely linked to large-scale changes in both MSLP and stratiform rainfall.

The FF ensemble suggests a shift of the high pressure belt farther south. The location is farther south than with the NNR but is not inconsistent in terms of mechanism. These anomalies drive the downscaling technique toward a rainfall decline in three out of four numerical simulations. The downscaled rainfall from the natural (Nat) ensemble shows quite a different pattern and does not match the observations. This indicates that the rainfall decline can be more readily attributed to the combination of natural and anthropogenic forcing. While the downscaling of the Nat ensemble does not provide any simulation that resembles observed changes, three members out of four of the FF ensemble reproduce a realistic, albeit underestimated, rainfall decline. This result suggests that although anthropogenic forcing is needed to explain the rainfall decline, the presence of anthropogenic forcing did not guarantee a rainfall decline overall.

The finding that GCM large-scale results need to be carefully analyzed to form the basis for regional climate change assessment is consistent with previous studies (Risbey et al. 2002). Indeed, the downscaling of the twentieth-century simulations provides a much clearer picture than the direct model rainfall can. The particular timing of the rainfall decline in the 1960s and 1970s, however, is not explained by our study. This may mean that either the forcing, the model, or the downscaling is imperfect or that other forcing types need to be considered. Among other factors, this particular behavior could be internally generated random long-term variability or external forcing, not included in our study, such as land clearance. It is recognized that the FF

ensemble does not encompass all of the known possible forcing of the climate system (e.g., indirect aerosol effect or land clearance are not included). It is worth pointing out, for example, that most land clearance in SWA occurred at about or before the time of the rainfall decline, in the 1950s to 1960s.

Acknowledgments. The authors are grateful to W. Drosdowsky, P. Hope, J. Risbey, and two anonymous reviewers for providing helpful comments to improve the original manuscript. We thank W. Washington, G. Meehl, and the NCAR group for making results from the PCM model available. Portions of this study were supported by the Office of Biological and Environmental Research, the U.S. Department of Energy as part of its Climate Change Prediction Program, and the National Science Foundation. Figure 1 was provided by P. Hope from BMRC. The first author is supported by a grant from the Australian Greenhouse Office.

REFERENCES

Allan, R. J., and M. R. Haylock, 1993: Circulation features associated with the winter rainfall decrease in southwestern Australia. *J. Climate,* **6,** 1356–1367.

Allen, M. R., and W. J. Ingram, 2002: Constraints on future changes in climate and the hydrological cycle. *Nature,* **419,** 224–232.

Benestad, R. E., 2004: Empirical–statistical downscaling in climate modeling. *Eos, Trans. Amer. Geophys. Union,* **85,** 417–422.

Bonan, G. B., 1996: A land surface model (LSM version 1) for ecological, hydrological and atmospheric studies: Technical description and user's guide. NCAR Tech. Note NCAR/TN-417+STR, National Center for Atmospheric Research, 150 pp.

Charles, S. P., B. C. Bates, P. H. Whetton, and J. P. Hughes, 1999: Validation of downscaling models for changed climate conditions: Case study of southwestern Australia. *Climate Res.,* **12,** 1–14.

Cubasch, U., and Coauthors, 2001: Projections of future climate change. *Climate Change 2001: The Scientific Basis*, J. T. Houghton et al., Eds., Cambridge University Press, 525–582.

Folland, C. K., and Coauthors, 2001: Global temperature change and its uncertainties since 1861. *Geophys. Res. Lett.,* **28,** 2621–2624.

Gentilli, J., 1972: *Australian Climate Patterns.* Nelson, 285 pp.

Gillett, N. P., F. W. Zwiers, A. J. Weaver, and P. A. Scott, 2003: Detection of human influence on sea-level pressure. *Nature,* **422,** 292–294.

——, A. J. Weaver, F. W. Zwiers, and M. F. Wehner, 2004: Detection of volcanic influence on global precipitation. *Geophys. Res. Lett.,* **31,** LI2217, doi:10.1029/2004GL020044.

Giorgi, F., M. R. Marinucci, and G. Visconti, 1990: Use of limited area model nested in a general circulation model for regional climate simulation over Europe. *J. Geophys. Res.,* **95,** 18 413–18 431.

Hewitson, B. C., and R. G. Crane, 1996: Climate downscaling: Techniques and application. *Climate Res.,* **7,** 85–95.

Imbert, A., and R. E. Benestad, 2005: An improvement of analog model strategy for more reliable local climate change scenarios. *Theor. Appl. Climatol.,* **82,** 245–255.

IOCI Panel, Eds., 1999: Towards understanding climate variability in south western Australia—Research reports on the first phase of the Indian Ocean Climate Initiative. Indian Ocean Climate Initiative Panel Tech. Rep. 1, Perth, Australia, 237 pp. [Available online at http://www.ioci.org.au/publications/pdf/IOCI_FPR_1.pdf.]

——, 2001: Towards understanding climate variability in south western Australia—Research reports on the second phase of the Indian Ocean Climate Initiative. Indian Ocean Climate Initiative Panel Tech. Rep. 2, Perth, Australia, 193 pp. [Available online at http://www.ioci.org.au/publications/pdf/IOCI_SPR.pdf.]

Jones, D. A., and G. Weymouth, 1997: An Australian monthly rainfall dataset. Bureau of Meteorology Tech. Rep. 70, 19 pp.

Kalnay, E., and Coauthors, 1996: The NCEP/NCAR 40-Year Reanalysis Project. *Bull. Amer. Meteor. Soc.,* **77,** 437–471.

Kiehl, J. T., J. J. Hack, G. B. Bonan, B. A. Boville, D. L. Williamson, and P. J. Rasch, 1998: The National Center for Atmospheric Research Community Climate Model: CCM3. *J. Climate,* **11,** 1131–1149.

Lambert, F. H., P. A. Stott, M. R. Allen, and M. A. Palmer, 2004: Detection and attribution of changes in the 20th century land precipitation. *Geophys. Res. Lett.,* **31,** L10203, doi:10.1029/2004GL019545.

Lavery, B., A. Kariko, and N. Nicholls, 1992: A historical rainfall data set for Australia. *Aust. Meteor. Mag.,* **40,** 33–39.

——, G. Joung, and N. Nicholls, 1997: An extended high-quality historical rainfall dataset for Australia. *Aust. Meteor. Mag.,* **46,** 27–38.

Lorenz, E. N., 1969: Atmospheric predictability as revealed by naturally occurring analogues. *J. Atmos. Sci.,* **26,** 636–646.

McAvaney, B. J., and Coauthors, 2001: Model evaluation. *Climate Change 2001: The Scientific Basis,* J. T. Houghton et al., Eds., Cambridge University Press, 471–523.

Meehl, G. A., W. M. Washington, T. M. L. Wigley, J. M. Arblaster, and A. Dai, 2003: Solar and greenhouse gas forcing and climate response in the twentieth century. *J. Climate,* **16,** 426–444.

——, ——, C. M. Ammann, J. M. Arblaster, T. Wigley, and C. Tebaldi, 2004: Combinations of natural and anthropogenic forcings in twentieth-century climate. *J. Climate,* **17,** 3721–3727.

Mitchell, J. F. B., D. J. Karoly, G. C. Hegerl, F. W. Zwiers, M. R. Allen, and J. Marengo, 2001: Detection of climate change and attribution of causes. *Climate Change 2001: The Scientific Basis,* J. T. Houghton et al., Eds., Cambridge University Press, 695–738.

Nicholls, N., 1989: Sea surface temperatures and Australian winter rainfall. *J. Climate,* **2,** 965–973.

Pitman, A. J., G. T. Narisma, R. A. Pielke Sr., and N. J. Holbrook, 2004: Impact of land cover change on the climate of southwest Western Australia. *J. Geophys. Res.,* **109,** D18109, doi:10.1029/2003JD004347.

Rayner, N. A., D. E. Parker, E. B. Horton, C. K. Folland, L. V. Alexander, D. P. Rowell, E. C. Kent, and A. Kaplan, 2003: Global analyses of sea surface temperature, sea ice, and night marine air temperature since the late nineteenth century. *J. Geophys. Res.,* **108,** 4407, doi:10.1029/2002JD002670.

Risbey, J. S., P. J. Lamb, R. L. Miller, M. C. Morgan, and G. H. Roe, 2002: Exploring the structure of regional climate sce-

narios by combining synoptic and dynamic guidance and GCM output. *J. Climate,* **15,** 1036–1050.

Santer, B. D., and Coauthors, 2003: Contributions of anthropogenic and natural forcing to recent tropopause height changes. *Science,* **301,** 479–483.

Schumacher, C., and R. A. Houze Jr., 2003: Stratiform rain in the Tropics as seen by the TRMM precipitation radar. *J. Climate,* **16,** 1739–1756.

Smith, I. N., P. McIntosh, T. J. Ansell, C. J. C. Reason, and K. McInnes, 2000: South–west Western Australia winter rainfall and its association with Indian Ocean climate variability. *Int. J. Climatol.,* **20,** 1913–1930.

Timbal, B., 2004: Southwest Australia past and future rainfall trends. *Climate Res.,* **26,** 233–249.

——, and B. J. McAvaney, 2001: An analogue-based method to downscale surface air temperature: Application for Australia. *Climate Dyn.,* **17,** 947–963.

——, A. Dufour, and B. J. McAvaney, 2003: An estimate of future climate change for Western France using a statistical downscaling technique. *Climate Dyn.,* **20,** 807–823.

Van den Dool, H. M., 1989: A new look at weather forecasting through analogues. *Mon. Wea. Rev.,* **117,** 2230–2247.

von Storch, H., 1999: On the use of "inflation" in statistical downscaling. *J. Climate,* **12,** 3505–3506.

Washington, W. M., and Coauthors, 2000: Parallel climate model (PCM) control and transient simulations. *Climate Dyn.,* **16,** 755–774.

Wright, P. B., 1974a: Seasonal rainfall in southwestern Australia and the general circulation. *Mon. Wea. Rev.,* **102,** 219–225.

——, 1974b: Temporal variations of seasonal rainfall in southwestern Australia. *Mon. Wea. Rev.,* **102,** 226–232.

Zhang, Y., and W. D. Hibler, 1997: On an efficient numerical method for modeling sea ice dynamics. *J. Geophys. Res.,* **102,** 8691–8702.